# Long range energy transfer in self-assembled stacks of semi-conducting nanoplatelets

*Jiawen Liu[1], Lilian Guillemeney[2], Benjamin Abécassis[2] and Laurent Coolen[1]*

*[1]Sorbonne Université, CNRS, Institut de NanoSciences de Paris, INSP, F-75005 Paris, France*

*[2]Univ Lyon, CNRS, École Normale Supérieure de Lyon, Laboratoire de Chimie UMR 5182, 46 allée d'Italie, F-69007 Lyon, France*

## Supporting information

### A – Synthesis and self-assembly of the nanoplatelets

*Materials :*

1-octadecene (90%) was purchased from Acros Organics. Selenium powder (99,5%), sodium oleate (82%), cadmium nitrate tetrahydrate (98%), cadmium acetate dihydrate, oleic acid (90%) were purchased from Sigma-Aldrich. Hexane (95%) was purchased from Fisher scientific. UV-vis absorption was measured on a Lambda 750 Perkin-Elmer spectrophotometer.

*Synthesis of cadmium oleate :*

Sodium oleate (12.1776 g, 40 mmol) is dissolved in a mixture of 200 mL of ethanol and 50 mL of water and then stirred at 45°C until getting a clear solution.

Cadmium nitrate tetrahydrate (6.1696 g, 20 mmol) is dissolved in 60 mL of ethanol at 45°C and added slowly to the sodium oleate solution with constant stirring and for 30 minutes at 45°C. The solution is allowed to cool down to room temperature and a sticking product is obtained. The solid product is then washed by successive centrifugations of 5 minutes at 3000 rpm (RCF = 916*g), twice by ethanol, three times by hot ethanol and once by hot methanol. The final beige product is dried under vacuum for one night.

*Synthesis of 5ML-CdSe NPL :*

Cadmium oleate (0.808 g, 1.20 mmol) is introduced with selenium powder (0.054 g, 0.68 mmol) and 30 mL of 1-octadecene (ODE) in a 50 mL-three-neck round bottom flask equipped with a septum, a temperature controller and an air condenser. The reaction mixture is degassed and kept under vacuum for 30 minutes. Afterward the flask is purged with argon and the temperature is set to 240°C. The rise in temperature has to occur quickly (6 or 7 minutes to heat up the reaction mixture from room temperature to 240°C). At 160°C the selenium begins to dissolve and the solution turns yellow. When the temperature reaches 205°C, the septum is withdrawn and cadmium acetate dihydrate (0.280 g, 1.05 mmol) is swiftly injected into the flask. The solution turns dark red. After the temperature reaches 240°C, the reaction is continued for 12 minutes. 1 mL of oleic acid is finally injected and the flask is immediately cooled down to room temperature using a water bath.

At this stage of the reaction, the mixture contains 5-ML CdSe NPL, 3ML-CdSe NPL and quantum dots in solution. The crude product is transferred in two 50 mL centrifuge tubes and 10 mL of acetonitrile is added in each tube which are then vortexed. The solution is centrifuged for 10 minutes at 6000 rpm (RCF = 3663*g). For each tube, the supernatant containing mainly quantum dots is discarded and the

solid precipitates containing NPL are dissolved in 20 mL of hexane. The resulting hexane solution is centrifuged 10 minutes at 6000 rpm (RCF = 3663*g) in order to remove the 3ML-CdSe NPL. The supernatant containing the 5ML-CdSe NPL is transferred in a new centrifugation tube and is washed by adding 10mL of ethanol in each tube. The tubes are centrifuged 10 minutes at 5000 rpm (RCF = 2543*g). The final solid product is dissolved in a total amount of 20 mL of hexane and its purity is verified by UV-vis absorption spectrometry and MET experiments. If there are still 3ML-CdSe NPL in solution, the hexane solution of 5ML-CdSe NPL could be centrifuged a last time for 15 minutes at 6000 rpm (RCF = 3663*g). The supernatant is then the final product.

*Self-assembly of 5ML-CdSe NPL :*

An appropriate amount of 5ML-CdSe NPL in hexane is diluted in hexane in order to get an absorbance at 552nm of approximately 2 (total volume of 2 mL (resp. 5mL)). Oleic acid (OA) is then added, such as the final concentration in OA in the sample is fixed between 0.025 mol/L and 0.05 mol/L and adjusted in order to get threads of different lengths. The sample is sonicated for 10 minutes and the solvent is slowly evaporated.

The solution was then diluted 500 times and spin-coated on a glass slide at 4000 rpm for 40 s. The sample was then covered by a 30-nm layer of PMMA.

*Center-to-center distance between the NPLs :*

The NPL center-to-center distance δ of a given chain was obtained from TEM images by averaging over around 50 platelets. This was repeated for 6 chains and an average value of δ = 5.69 nm was measured with 0.02-nm standard deviation. Another method is to use small-angle X-ray scattering[10]. The distance between the NPL corresponds to $2\pi/q^*$ where $q^*$ is the scattering vector of the first order Bragg peak in the scattering pattern. We then find a distance of 5.84 nm. Finally, we have performed similar measurements on high resolution STEM images acquired in HAADF mode (fig. S1). In this case, we found a δ=4.75 nm. We thus have different delta values depending on the way to measure it. We believe the differences between these values may be due to the level of vacuum in which the measurements are performed. In the case of SAXS, the measurement is performed in solution and solvent molecules can be present between the NPL thus increasing the distance between them. In the TEM, the measurements are performed in vacuum. This can have two effects: expand the organic molecules but also evaporate all the solvent molecules between the NPL and thus decrease the distance. The level of vacuum being different between the STEM and TEM measurements (higher vacuum in the case of STEM) it is not surprising to observe differences in the distances between the two measurements. These experiments show that the largest uncertainty on the delta value comes from this and not from a spread in the actual value of delta in a given sample which is small. As a matter of fact, the center to center distance is dictated by the thickness of the NPL which is known to be homogeneous at the atomic scale and the length of the ligand which is also very well defined. During our optical measurements we are in an intermediate case since we performed the measurements under ambient pressure but after the evaporation of the solvent. We will take the intermediate value 5.7 nm as an estimate of the distance $\delta$ for the discussion of our microscopy observations.

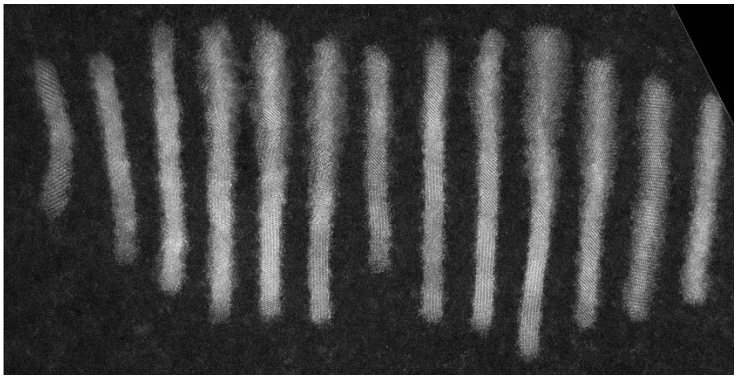

*Figure S1 : High-resolution HAADF image of a CdSe NPL stack*

The twisting of the NPL is not expected to impact the center to center distance since we observe on the STEM images that the twisting is correlated between two neighbor NPL. This is also confirmed by SAXS experiments where the position of the peak did not vary with time during the different steps of the assembly process (fig. S2 in our ref. 10). We observed that the distance between NPL is the same during the early steps of the assembly when there is no twist and during the next steps when the twist occurs and the range of the assembly is increasing.

**B - Photoluminescence of single platelets**

*Emission spectra :*

The spectra of single platelets are recorded by a monochromator (Triax 190 @Horiba) under pulsed laser excitation at 2.5-MHz repetition rate with input power of 10-nW and acquisition duration 20 s. Fig. S2(a) shows 4 examples of single platelet's spectrum while S2(b) summarizes the central wavelength and emission line width of 11 single platelets. The emission wavelengths of the platelets are typically 549 nm with negligible dispersion, showing the excellent homogeneity of the sample and excluding any strong hetero-FRET effect. The reason for the negligible inhomogeneity is that the exciton energy depends only on the vertical confinement and that the NPL thickness is controlled with atomic-layer precision in the synthesis process.

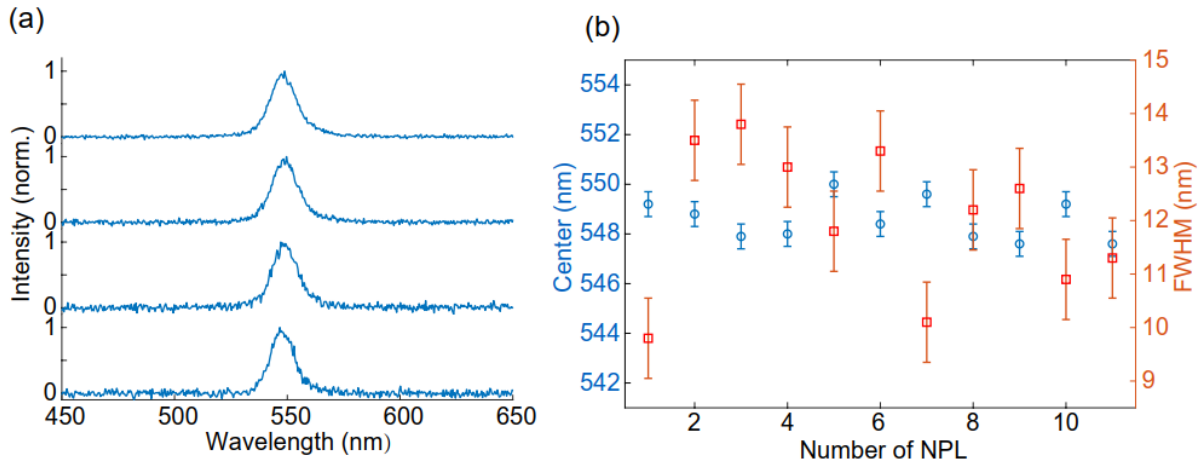


*Figure S2 : (a) spectra of 4 single platelets; (b) emission wavelength and peak FWHM of 11 single platelets.*

*Decay curves :*

The pulsed laser is set at 2.5-MHz repetition rate with input power of 7-nW. A fast time correlated single-photon counting module combined with PicoHarp acquisition card are employed for decay curve measurements with 500-ps characteristic time of the total system response function.

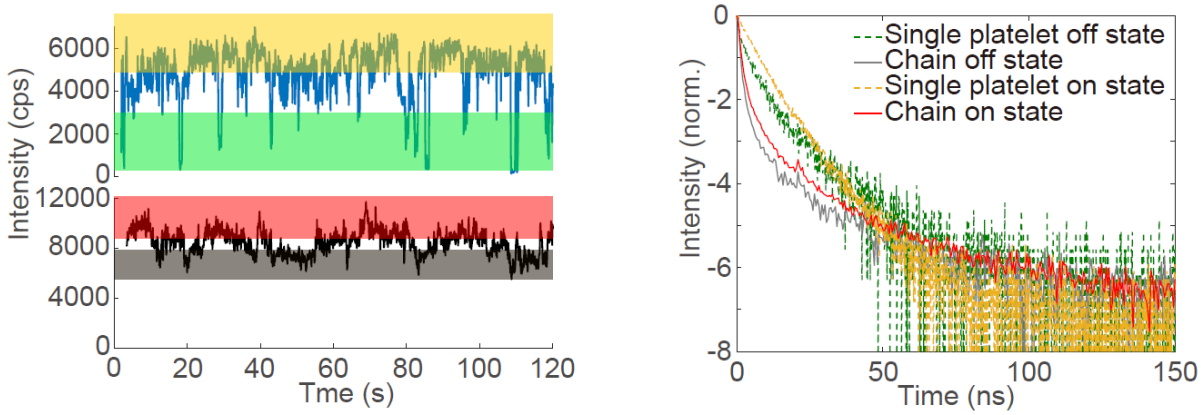


*Figure S3 : Left : Intensity time traces of single platelet (blue) and platelet chain (black); the selected on-state and off-state emission ranges are indicated by different shades. Right : Decay curves of on-state (yellow/red) and off-state (blue/black) emission of single platelet/chain (excitation power 7 nW).*

The decay curve of semi-conductor nanoparticles is well-known to be affected by blinking (random switching between luminescent “on” and non-luminescent “off” states. An example is shown in fig. S3 for a single NPL and for a NPL chain by plotting the decay curves of either “on” or “off states (for the chain, the “off” state corresponds to less-luminescent periods). For both types of emitters, the decay curves are faster for the “off” state because of non-radiative exciton recombination channels. We thus will plot decay curves of selected “on” states only in order to avoid adding irrelevant blinking effects to our analysis.

Figure S4(a) shows a typical decay curve of a single platelet (red) ; it is mostly monoexponential with a typical 10-ns decay time, suggesting very low non-radiative mechanisms and high quantum yield. As a point of comparison, we also plot the decay curve of a NPL chain (blue). The observed decay acceleration with respect to single NPLs is consistent with previously-reported observations on stacked NPLs[1,11,12] and NPL ribbons[13]. It has been attributed to the presence of defect NPL acting as collective quenchers[1, 11,13] : excitons in neighbor platelets are transferred by FRET to the defect platelet where fast non-radiative decay occurs.

To analyze quantitatively the decay curves, we use a four-exponential model to fit the data and deduce the amplitude-averaged lifetime :

$$\bar{\tau} = \frac{\sum {\tau_i}^2 \cdot A_i}{\sum \tau_i \cdot A_i}$$

where $A_i$ and $\tau_i$ represent the amplitude and characteristic time of the $i^{th}$ exponential component, respectively. We analyze the decay curves of 8 different single platelets. As shown in Fig. S4(b), we obtain a lifetime distribution with an averaged value of 12 ns, which can be assumed to correspond to the radiative decay time, and a standard deviation of 2.7 ns. Such an inhomogeneity in decay times is typical with semi-conductor nanoparticles, it may have different causes such as local electric fields or inhomogeneity of the oscillator strength due to the dispersion of lateral dimensions.

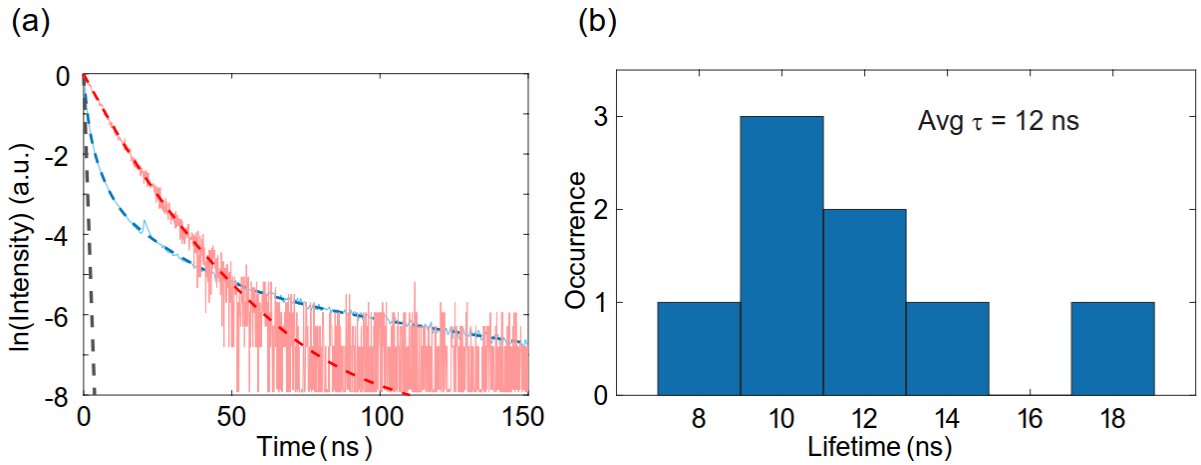


*Figure S4 : (a) Decay curves of single platelets (red) and stacked NPLs (blue). The grey dashed line indicates the instrument response function. (b) Distribution of single-platelet lifetimes.*

*Polarization analysis :*

Nanoplatelets are known to present two in-plane dipoles oriented along their long and short axes, respectively[3]. We analyzed in fig. S5 the polarization of the emission by rotating a polarizer in front of an avalanche photodiode detector, following the protocol described in ref. 3. We compared three excitation polarizations : either circular, linear along the long or the short axis. For the three orientations, the maximum detection was at analysis angle of 15 ± 2° and the degree of polarization was 0.37 ± 0.01. The emission polarization is thus not dependent on the excitation polarization.

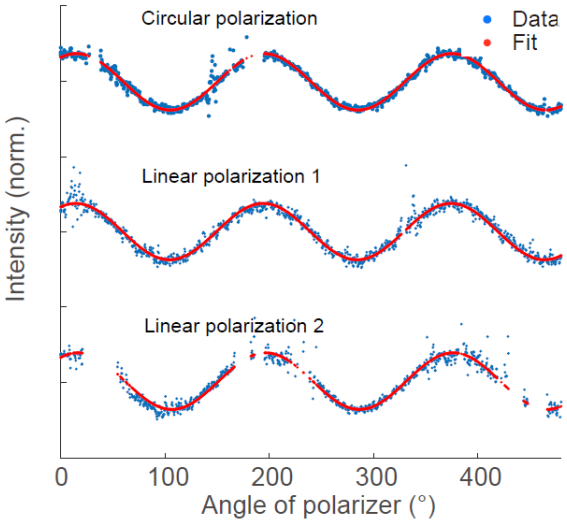


*Figure S5 : Emission polarization analysis of the same platelet under different excitations : circular (upper panel) or linear excitation along long (middle panel) or short (lower panel) axis of platelet.*

**C - Microphotoluminescence imaging and spatial resolution**

*Setup description :*

The experiments were performed on a homemade inverted fluorescence microscope equipped with laser scanning system. The excitation source could be either a mercury lamp (for wide field detection) or a 470 nm diode laser (PDL 800-D PicoQuant, 70-ps pulses, 2.5-MHz rate). The same objective (Olympus apochromat 100X 1.4N.A.) was used to focus the excitation beam on the sample and collect the emission. The scattered excitation light was filtered by a set of filters. The image was focused onto a charge-coupled device (QImaging Retiga EXi, pixel size 6.45 µm). The imaging magnification was 90 so that each pixel on the camera corresponded to 72 nm on the sample.

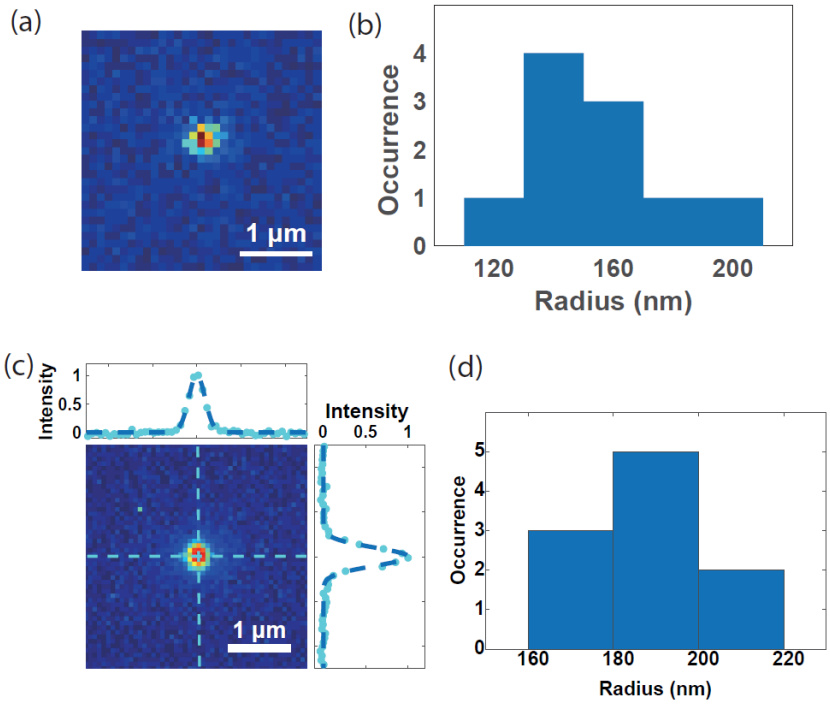


*Figure S6 : (a) confocal microscopy scan of a single nanoplatelet (scanning step 100 nm), (b) histogram of laser spot radii $r_L$ obtained by this method. (c) Image of a single NPL under wide field illumination on the camera (pixel size 72 nm on the sample), (d) histogram of point spread function radii $r_{PSF}$ obtained by this method.*

*Size of the laser excitation spot :*

We scanned a single nanoplatelet with a piezo-electric stage and detected its emission with avalanche photodiodes. A typical scan is shown in figure S6(a). Considering that the nanoplatelet size is negligible, the obtained image is a probe of the laser spot intensity on the sample. Its profile is well fitted by a Gaussian of the form $e^{-(x/r_L)^2}$. Figure S6(b) plots a histogram of the values of $r_L$ obtained by repeating this process several times. The average value of $r_L$ was 157 nm.

*Imaging system point spread function :*

Figure S6(c) displays a CCD camera image of a single nanoplatelet under wide field (Hg lamp) excitation. Considering the platelet as an emitter of negligible size, the obtained image is the point spread function of the detection part of the setup. Its profile is well fitted by a Gaussian of the form $e^{-(x/r_{PSF})^2}$. Figure S6(d) plots a histogram of the values of $r_{PSF}$ measured by repeating this process several times. The average value for $r_{PSF}$ was 190 nm.

*Overall system's response function in the experiment of figure 2 :*

If we consider the NPL chain as a one-dimensional line along axis $(Ox)$, the excited emitters are distributed along this line with an emission intensity proportional (in the linear excitation regime) to the laser spot intensity. In other words, *if no energy migration occurs*, the emission distribution should scale as $(y)e^{-(x/r_L)^2}$ : all emitters are along $(Ox)$, within a typical distance $r_L$ from the center of the laser spot. The image of these emitters is convolved by the system's point spread function in both $x$ and $y$ directions so that the final image scales as $e^{-(y/r_{PSF})^2}e^{-x^2/({r_L}^2+{r_{PSF}}^2)}$. Eventually, we expect that

- the profile of the detected image along $(Oy)$ (axis orthogonal to the chain) has a width $r_{PSF}$ = 190 nm ;
- while, if there is no energy migration within the chain, the profile along $(Ox)$ (parallel to the chain) has a width caused by the response function : $r_{RF} = \sqrt{{r_L}^2 + {r_{PSF}}^2}$ = 246 nm because the overall response function is a combination of the laser spot size and the imaging PSF.

  The fact that the measured width along $(Ox)$ axis has a width $l_x$ larger than $r_{RF}$ (fig. 3) is proof that there is energy migration along the thread. The FRET migration can be obtained by deconvolving the measured image by the influence of the setup's RF : $l_{FRET} = \sqrt{{l_y}^2 - {l_{RF}}^2}$.

**D - Waveguiding**

Here we evaluate whether the energy migration along the chain could be just caused by waveguiding of either the excitation or the emitted light within the chain.

*Model :*

Lumerical FDTD solution is employed to conduct this simulation. We build nanoplatelets with index[2] of 2.64+0.44i and dimension of 20 x 10 x 1.5 nm$^3$ sandwiched by ligand layers (index = 1.46, thickness 4.2 nm) to form a 500-nm long co-facially stacked structure (as shown in the schematic). A 750-nm long 500-nm wide monitor is positioned 30 nm under the stacks to properly collect all the near field electromagnetic waves. We also simulate the reference case without thread (only one platelet is located at $x = 0$). What we display on fig. S7 is the normalized difference $\left(\left|\vec{E}\right|^2 - \left|\vec{E}_{ref}\right|^2\right) / \left|\vec{E}_{ref}\right|^2$ in order to quantify the effect of waveguiding.

*Waveguiding of the excitation beam :*

A preliminary experimental answer is obtained by imaging the laser spot on the chain, this time without filtering out the 470-nm (laser) wavelength (fig. S7(a)). The obtained image, as compared to the luminescence image (also on fig. S7(a), obtained by selecting only the 550-nm emission wavelength), shows a clear circular shape, with no sign of propagation of the laser light along the thread.

This is confirmed on fig. S7(b) by simulating the electromagnetic field impinging on one end of the chain, with polarization either longitudinal or lateral with respect to the chain axis. For both excitation polarizations, the waveguiding effect is clearly visible, but its normalized relative value remains below 1 % along the whole chain.

*Waveguiding of the emitted photons :*

We show in fig. S7(c) the electric field radiated by a dipole inside a chain of platelets, with dipole orientation along either direction in the platelet plane (as it is known that emitting dipoles in such a platelet are parallel to the platelet plane[3]). Again, the waveguiding effect is clearly visible, but its normalized value remains within a few % along the whole chain.

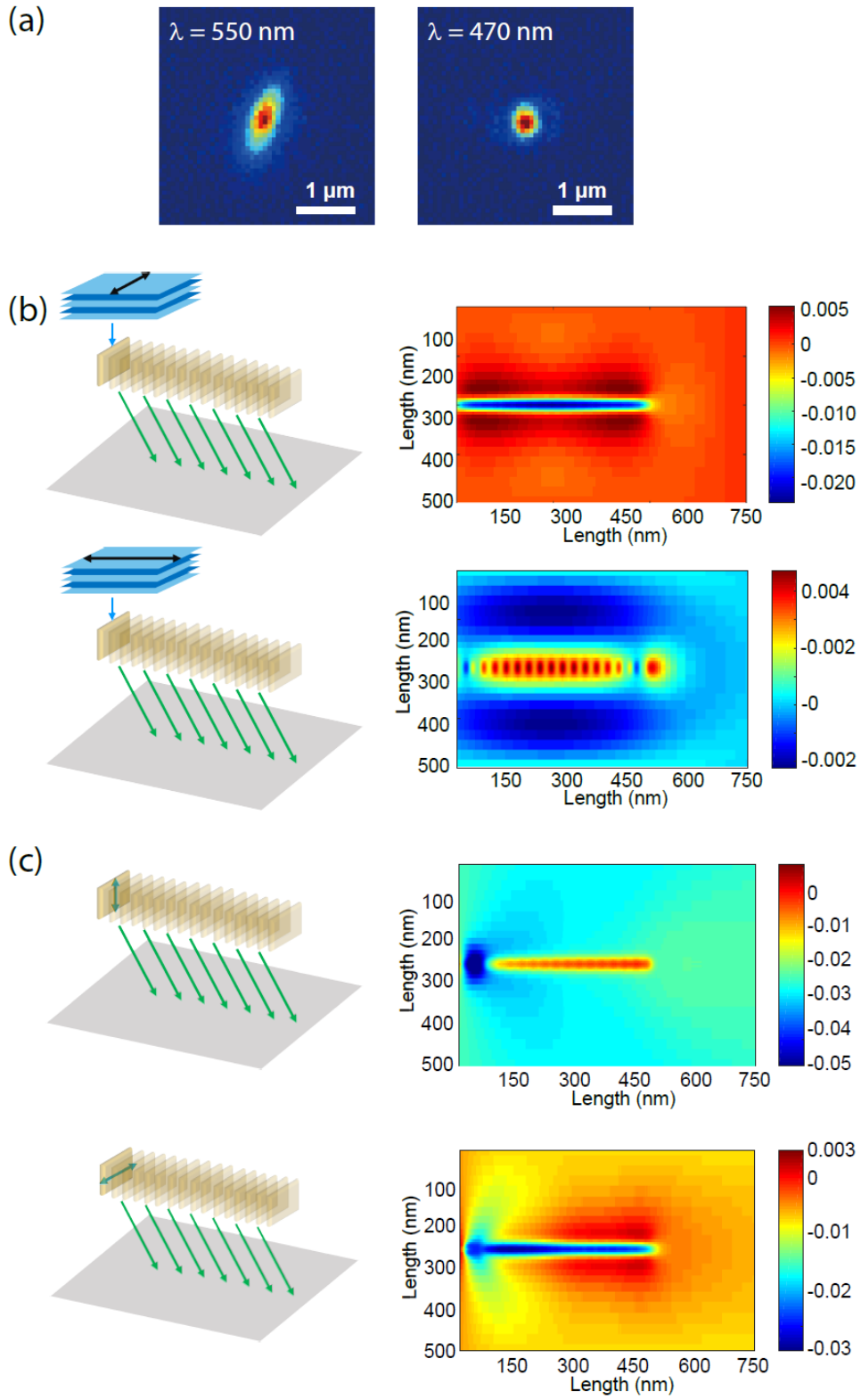


*Figure S7 : (a) Experimental analysis of the waveguiding effect of the excitation beam. (b) FDTD simulations of the waveguiding of the incident beam (plane wave, 470 nm) along the two horizontal polarizations. (c) FDTD simulations of the waveguiding of the emitted wave, with the dipole source of either orientation along the platelet plan, positioned at the first platelet (x = 0) of the chain which is 500nm in length (from x=0 to x=500).*

**E - Effect of excitation power**

The measurements in figures 2 and 3 (except 3(e)) were performed at around 5-nW excitation power. We now check that the chosen power was within the chain's linear regime and analyze the effect of the excitation power.

*Linear excitation regime of* single *platelets :*

We first ensure that the laser power is within the linear excitation regime of the NPLs in order to avoid multi-excitonic effects within a given platelet. We excite the same platelet emitter with various input powers and record its power-dependent intensity curve (fig. S8 (a)) and decay curves (fig. S8(b)) (for both (a) and (b) we select only the on-states in order to exclude blinking effects from the power-dependence analysis). The emission intensity increases linearly with the pump power within the range from 1.5 to 10-nW. When the excitation power varies between 1.5 and 10-nW, the decay dynamics of the selected on-state emission of the platelet also remain unchanged, confirming the absence of multiexcitonic contribution and nonlinear effects.

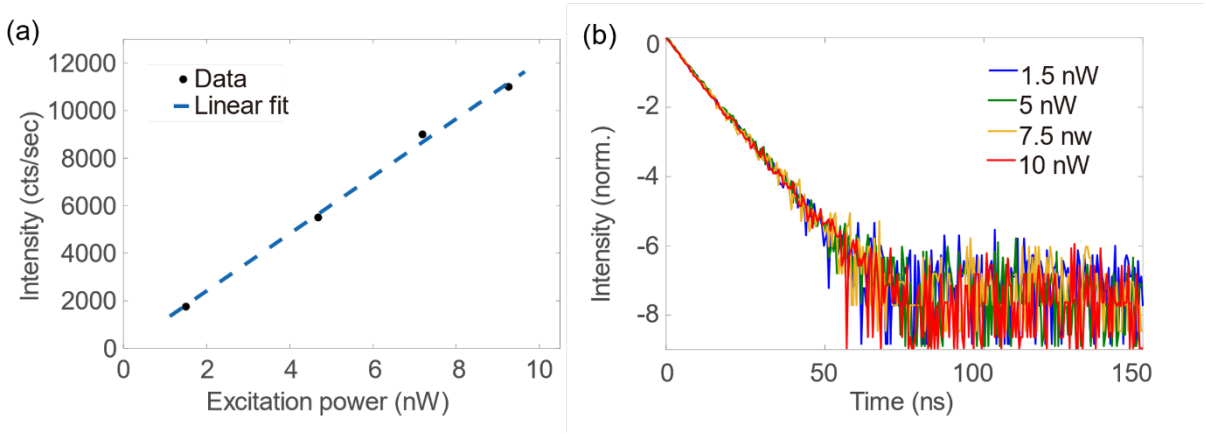


*Figure S8 : Power-dependent intensity curve (a) and decay curves (b) of a same single nanoplatelet (NPL) emitter under different excitation powers.*

At 5-nW excitation power fig. S8(a) shows around 6000 photon detections per second. We calculate, for these emitters on a glass slide imaged with a 1.4 oil objective, a photon collection efficiency around 80 %. Taking into account the overall setup transmission of 70 % and the photodiode detection efficiency of 55 % at 550 nm, a single NPL emits around 19 000 photons per second. The laser pulse rate is 2.5 MHz, so that each laser pulse leads to $8.10^{-3}$ photon emitted per laser pulse. We can assume, especially looking at the slow decay curves of single NPLs, that the NPL quantum yield is not too far from unity. Ref. 1 has reported a 30-% quantum yield for instance for cuvette measurement, but since we are here post-selecting only the on-states which have a slow monoexponential decay, we can assume the quantum yield to be close to 100 %. This would then mean that the number of excitons created per laser pulse is $8.10^{-3}$ at 5-nW excitation. We are indeed well below the nonlinear regime, in agreement with the observations of fig. S8.

Given the laser pulse rate of 2.5 MHz and wavelength of 470 nm, at 5 nW each laser pulse corresponds to 4700 incident photons. From ref. 6, where the absorption cross section was measured as a function of the NPL area, we may estimate for our NPL size the maximal absorption cross-section as $\sigma = 7.10^{-14}$ cm² and from the absorption spectrum in fig. 1(b) deduce around $\sigma = 5.10^{-14}$ cm² at 470 nm.

Approximating the laser spot as a disk of radius 160 nm, we find at 5 nW that each pulse should lead to 0.3 photon absorption for a single NPL under 5-nW excitation. This number is extremely high as compared to the measured $8.10^{-3}$ photon emitted per pulse. It might be attributed to an extremely low quantum yield, but this seems unlikely given the monoexponential shape of the decay curves. It seems more likely that such an estimation of the number of absorbed photons relies on too many approximations to be accurate ; possibly the absorption cross-section value is not appropriate here.

*Number of photons emitted per laser pulse by a NPL chain :*

For a NPL chain under 5 nW excitation, count rates ranging between $10^4$ and $10^5$ photon/sec. were measured, which following the above considerations leads to 0.01-0.12 photon emitted per laser pulse. Again, this would correspond to a number of excitons per pulse in the entire chain lower than unity, except if the quantum yield is very low.

We can estimate that a portion of the chain of 320 nm (diameter of the laser spot) is excited, corresponding to 55 platelets. This would lead to around $(0.2\text{-}2).10^{-3}$ photon emitted per pulse and per NPL in the chain. This is much lower than the $8.10^{-3}$ photon emitted per pulse by the single NPL. One reason can be that the stacked platelets are vertical while the single platelets deposit horizontally, so that their absorption cross-section should be lower when stacked. Another effect is the reduced quantum yield in stacks due to exciton FRET-mediated funneling to quenchers (defect NPLs)[1]. It seemed during our experiments that some sample depositions provided generally higher emission than others, which could be an indication of the effect of sample preparation (sonication for instance) on the general quantum yield of the stacked NPLs.

If we assume the number of excitons created per pulse in each NPL to be the same as in single NPLs, our value of $8.10^{-3}$ exciton/pulse at 5-nW excitation would correspond to 0.44 exciton/pulse in the entire chain. It might in fact be lower because, as mentioned above, the platelets are vertical in the chain and should be excited less efficiently. We thus expect our measurements to be performed with less than one exciton per pulse in the chain and avoid multi-excitonic effects (as is confirmed experimentally by the absence of power-dependence in fig. 3(e)).

*Power-dependent decay dynamics of platelet chain*

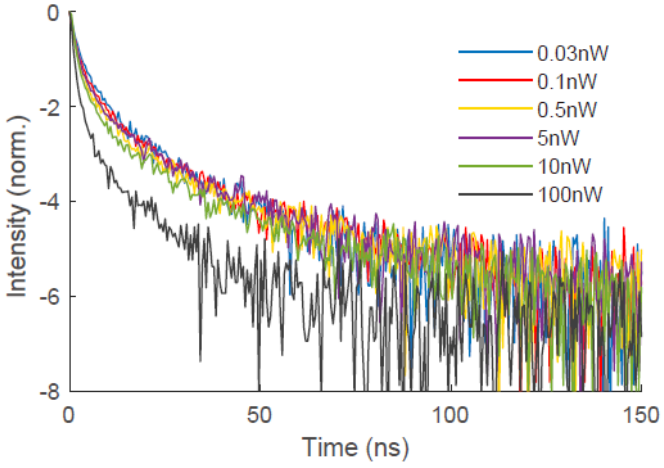


*Figure S9 : decay curves of a same platelet chain under different excitation powers.*

We excite a same platelet chain with different input powers and record its power-dependent decay curves (fig. S9). A variable neutral density filter is used to keep a constant photon detection rate (around $10^3$ counts/sec) in the avalanche photon detector. When the excitation power varies from 0.03 to 5-nW, which covers the typical power range that was used in the platelet chain measurements, the decay dynamics of the chain remain unchanged, confirming the absence of nonlinear effects. At 10-nW (which starts to exceed the power range used in the measurements), the decay rate slightly changes and then it significantly accelerates at 100 nW. The measurements were performed under 5-nW excitation, within the range where the decay shows little power dependence. The faster decay at 100-nW excitation may be due either to multi-excitonic effects such as exciton-exciton Auger annihilation or to quenching mechanisms. Further measurements beyond the scope of this paper will be necessary to precise the mechanism of non-linear effects at these powers.

**F - Diffusion model**

*Model :*

We assume that the chain length is infinite and we introduce a center-to-center nanoplatelet distance $\delta$, a transfer rate between neighbor platelets $\gamma_{tr}$ and an exciton decay rate $\gamma_0$ which is a sum of respectively radiative and non-radiative decays rates $\gamma_{rad}$ and $\gamma_{nr}$ (these quantites being assumed the same for all platelets). If an exciton is created at time $t = 0$, the probability $n_i$ that the $i^{th}$ platelet is excited obeys :

$$\frac{dn_i}{dt} = -(\gamma_0 + 2\gamma_{tr})n_i + \gamma_{tr}(n_{i-1} + n_{i+1})$$

When considering length scales much larger than $\delta$, one may refer to each platelet by its position $x$ and introduce the exciton probability density $n(x,t)$. We note that

$$\frac{\partial^2 n}{\partial x^2} \approx \frac{n_{i+1} + n_{i-1} - 2\,n_i}{\delta^2}$$

so that we obtain the standard diffusion equation (with an additional loss term due to $\gamma_0$) :

$$\left(\frac{\partial n}{\partial t}\right)(x,t) = -\gamma_0\ n(x,t) + D\left(\frac{\partial^2 n}{\partial t^2}\right)(x,t)$$

with the diffusion coefficient $D = \delta^2\gamma_{tr}$.

*Solution :*

Because this is a linear equation with translational invariance, our discussion can be limited to the case where a single exciton is introduced at $t = 0$ at the position $x = 0$. This corresponds to a Dirac distribution for $n(x, t = 0)$, with the normalization condition $\int_{x=-\infty}^{+\infty} n(x, t = 0)dx = 1$. The solution of this equation is :

$$n(x,t) = \frac{1}{2\sqrt{D\pi t}} e^{-\frac{x^2}{4Dt}} e^{-\gamma_0 t}$$

The exciton probability distribution combines a typical diffusive broadening of width $2\sqrt{Dt}$ with a general decrease as $e^{-\gamma_0 t}$ due to the recombination losses.

*Decay curve of the overall chain :*

The photon emission rate of the overall chain is given by

$$I_{decay}(t) = \int \gamma_{rad} n(x,t) dx$$

Integration of $n(x,t)$, a Gaussian function of $x$, leads to :

$$I_{decay}(t) = \gamma_{rad} e^{-\gamma_0 t}$$

The same result would also be obtained by integrating directly the diffusion equation over $x$. Its meaning is that the homo-FRET diffusion term redistributes the excitons within the thread, but the decay term $\gamma_0$ is the only one responsible for a decrease of the total number of excitons.

Migration by homo-FRET differs from the hetero-FRET mechanism as only one jump can occur in the latter so that FRET rate can be extracted from hetero-FRET decay curves. However, for hetero-FRET between stacked platelets of different thicknesses, very different FRET rates ranging from 10 ps to 1 ns have been reported[7-8]. The inconsistency between these values might be due to insufficient control of the stacking order[9].

*Luminescence image of the thread :*

The image of the thread is obtained by summing the probabilities of photon emission from a given point $x$ over all times $t$ :

$$I(x) = \int_{t=0}^{+\infty} \gamma_{rad} n(x,t) dt$$

(the imaging point spread function is not included in this description).

One can find $I(x)$ by noting that

$$\frac{dI}{dx} = \frac{\gamma_{rad}}{2\sqrt{D\pi}} \int_{t=0}^{+\infty} \frac{dt}{\sqrt{t}} \frac{(-x)}{2Dt} e^{-\left(\frac{x^2}{4Dt} + \gamma_0 t\right)}$$

which, by introducing $u = x^2/4D\gamma_0 t$, rewrites (for $x > 0$)

$$\frac{dI}{dx} = \sqrt{\frac{\gamma_0}{D}} \frac{\gamma_{rad}}{2\sqrt{D\pi}} \int_{u=+\infty}^{0} \frac{du}{\sqrt{u}} e^{-\left(\frac{x^2}{4Du} + \gamma_0 u\right)}$$

where we recognize

$$\frac{dI}{dx} = -\sqrt{\frac{\gamma_0}{D}}\, I$$

By introducing $l_{FRET} = \sqrt{D/\gamma_0}$ , and having calculated that $I(0) = \gamma_{rad}/2\gamma_0 l_{FRET}$ , we find eventually

$$I(x) = \frac{\gamma_{rad}}{2\gamma_0 l_{FRET}}\, e^{-|x|/l_{FRET}}$$

*Total number of emitted photons :*

We have assumed that a single exciton is introduced at $t = 0$. The number of photons emitted can be obtained either by integrating $I_{decay}(t)$ or by integrating $I(x)$. Both summations lead to the total

number of photons emitted (probability for photon emission when one exciton is introduced) : $\gamma_{rad}/\gamma_0$. This probability is none other than the quantum yield of individual platelets : even though FRET redistributes the energy along the thread, the radiative decay and total decay of the overall thread are the same as the decays for a single platelet.

**G - FRET rate theoretical estimate :**

The rate of FRET between two identical dipoles oriented respectively along unit vectors $\overrightarrow{n_D}$ and $\overrightarrow{n_A}$, separated by a distance $\delta$, is given by Förster's equation[5] :

$$\gamma_{tr} = \gamma_0 \left(\frac{R_0}{\delta}\right)^6$$

where $\gamma_0$ is the radiative decay rate and $R_0$ is Förster's radius :

$${R_0}^6 = \frac{9c^4\kappa^2}{8\pi}\int_{\omega=0}^{\infty} \frac{f_D(\omega)\sigma_A(\omega)}{n^4(\omega)\omega^4}\,d\omega$$

In this equation, $n$ is the homogeneous surrounding medium's index, $f_D(\omega)$ is the emission spectrum normalized by $\int f_D(\omega)d\omega$ = 1 and $\sigma_A$ is the absorption cross section. The orientation factor $\kappa$ is defined as

$$\kappa^2 = \left(\overrightarrow{n_A}.\overrightarrow{n_D} - 3(\overrightarrow{n_R}.\overrightarrow{n_D})(\overrightarrow{n_R}.\overrightarrow{n_A})\right)^2$$

where $\overrightarrow{n_R}$ is the unit vector from the donor to the acceptor. For parallel platelets, the dipoles are along the plane of the platelets[3] so that $\overrightarrow{n_R}.\overrightarrow{n_D} = 0$ and $\overrightarrow{n_R}.\overrightarrow{n_A} = 0$. Let us consider parallel dipoles (as orthogonal dipoles would have no coupling) : then $\kappa^2 = 1$.

Let us also simplify the equation by considering that the emission line is sufficiently sharp that $n^4(\omega)\omega^4$ can be considered constant over the emission spectrum. Then Förster's radius can write :

$${R_0}^6 = \frac{9}{8\pi}\left(\frac{\lambda}{2\pi n}\right)^4 \int f_D(\omega)\sigma_A(\omega)d\omega$$

We take $\lambda$ = 550 nm, $n$ = 1.5 and we use our experimental emission spectrum for $f_D(\omega)$ (fig. 1(b)). We find $\sigma_A(\omega)$ as $\sigma_0 u(\omega)$ where $u(\omega)$ is our measured absorption spectrum (normalized by $u = 1$ at the maximum). The maximal absorption cross-section is estimated to $\sigma_0$ = $7.10^{-14}$ cm² from ref. 6 where the absorption cross-section was calibrated as a function of the NPL area. We find eventually $R_0$ = 17 nm, so that, with the radiative decay time 12 ns and the distance $\delta$ = 5.7 nm, we conclude for the FRET time : $(1/\gamma_{tr})$ = 17 ps.

**H – Laser excitation at the end of the chain**

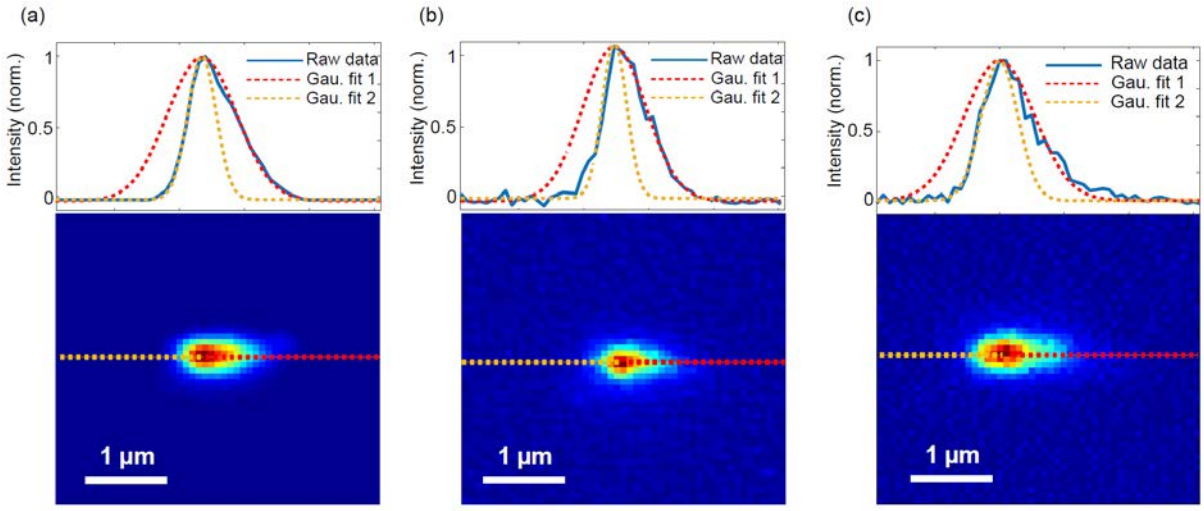


*Figure S10 : Profiles of 3 representative NPLs chains with excitation on their edge. The blue solid line is the experimental profile. The red and yellow dotted lines correspond to gaussian fits of respectively the right and left portions of the experimental curve.*

Figure S10 shows the luminescence image of three different NPL chains measured under the same conditions as in fig. 2(b), except that the laser excitation spot was positioned at the end of the NPL chain instead of the center. For the first 2 chains, the left portion of the profile curve was fitted by a Gaussian (yellow curve) of respective widths 223 and 194 nm, which corresponds to the imaging response function $r_{PSF}$ = 190 nm measured in section S.I.-C. The right side of the curve was fitted with a Gaussian (red curve) of width respectively 543 and 504 nm, similar to the widths $l_x$ reported in fig. 3(c), so that a FRET diffusion length of 484 and 440 nm can be extracted. For the 3$^{rd}$ chain, the left portion extended slightly longer (252-nm Gaussian width), possibly because the laser spot was not exactly at the end of the chain, but the estimated FRET length on the right portion was 496 nm, in the same range as chains (a) and (b) and fig. 3(d).

**References :**

[1] B. Guzelturk, O. Erdem, M. Olutas, Y. Kelestemur and H. V. Demir, Stacking in colloidal nanoplatelets : tuning excitonic properties, ACS Nano 8, 12524 (2014),

[2] S. Ninomiya and S. Adachi. Optical properties of cubic and hexagonal CdSe, J. Appl. Phys. 78, 4681 (1995),

[3] F. Feng, L. T. NGuyen, M. Nasilowski, B. Nadal, B. Dubertret, L. Coolen and A. Maître, Consequence of shape elongation on emission asymmetry for colloidal CdSe/CdS nanoplatelets, Nano Research 11, 3593 (2018),

[4] W. D. Kim, D. Kim; D.-E. Yoon, H. Lee, J. Lim, W. K. Bae and D. C. Lee, Pushing the efficiency envelope for semiconductor nanocrystal-based electroluminescence devices using anisotropic nanocrystals, Chem. Mater. 31, 3066 (2019),

[5] Lukas Novotny and Bert Hecht, Principles of Nano-Optics, Cambridge University Press, Cambridge (United Kingdom, 2006),

[6] A. Yeltik, S. Delikanli, M. Olutas, Y. Kelestemur, B. Guzelturk and H. V. Demir, Experimental determination of the absorption cross-section and molar extinction coefficient of colloidal CdSe nanoplatelets, J. Phys. Chem. C 119, 26768 (2015),

[7] C. E. Rowland, I. Fedin, H. Zhang, S. K. Gray, A. O. Govorov, D. V. Talapin and R. D. Schaller, Nature Materials 14, 484 (2015),

[8] B. Guzelturk, M. Olutas, S. Delikanli, Y. Kelestemur, O. Erdem and H. V. Demir, Nonradiative energy transfer in colloidal CdSe nanoplatelet films, nanoscale 7, 2545 (2015),

[9] B. Guzelturk and H. V. Demir, Near-field energy transfer using nanoemitters for optoelectronics, Adv. Funct. Mater. 26, 8158 (2016),

[10] S. Jana, M. de Frutos, P. Davidson and B. Abécassis, Ligand-induced twisting of nanoplatelets and their self-assembly into chiral ribbons, Sci. Adv. 3:e1701483 (2017),

[11] A. Antanovich, A. Prudnikau, A. Matsukovich, A. Achtstein and M. Artemyev, Self-assembly of CdSe nanoplatelets into stacks of controlled size induced by ligand exchange, J. Phys. Chem. C 120, 5764 (2016),

[12] Y. Gao, M. C. Weidman and W. A. Tisdale, CdSe nanoplatelet films with controlled orientation of their transition dipole moment, Nano Lett. 17, 3837 (2017),

[13] W. D. Kim, D.-E. Yoon, D. Kim, S. Koh, W. K. Bae, W.-S. Chae and D. C. Lee, Stacking of colloidal CdSe nanoplatelets into twisted ribbon superstructures, J. Phys. Chem C 123, 9445 (2019).